Supplementary Information

Quantifying the tuneable interactions between colloid supported lipid bilayers

Materials and methods

Materials

Phospholipids 1,2-dioleoyl-sn-glycero-3-phosphocholine (DOPC), 1,2-dipalmitoyl-sn-glycero-3-phosphocholine (DPPC), PEGylated lipid 1,2-distearoyl-sn-glycero-3-phosphoethanolamine-N-[methoxy(polyethylene glycol)-2000] (DSPE-PEG$_{2000}$), and dye-conjugated lipids 1,2-dioleoyl-sn-glycero-3-phosphoethanolamine-N-(lissamine rhodamine B sulfonyl) (DOPE-rhod), 1,2-dipalmitoyl-sn-glycero-3-phosphoethanolamine-N-(lissamine rhodamine B sulfonyl) (DPPE-rhod) were purchased from Avanti Polar Lipids, USA. The PEGylated lipid DSPE-PEG$_{2000}$ contains a PEG chain with a molar mass M = 2000 kDa comprising 45 monomers with a monomer molar mass M_{mon} = 44,05 kDa. 100 kDa poly(ethylene oxide), with a degree of polymerization, DP = $M_{\mathrm{PEG}}/M_{\mathrm{mon}}$ = 2270, was purchased from Sigma Aldrich.

Methods

SUVs of DOPC and DPPC were formed via thin film hydration and extrusion with a 100 nm membrane filter above the phase transition temperature (T_{m}) of the phospholipids, -17 °C and 41 °C, respectively. To provide fluorescence to the bilayer, 1 mol% of dye-conjugated phospholipid was included. Specifically, DOPE-rhod for DOPC CSLBs and DPPE-rhod for DPPC CSLBs were used. CSLBs composed by fluid or gel phospholipids, with varying amounts of membrane bound PEGylated lipid, were synthesised by rupture and fusion of SUVs onto 3 μm silica particles. A buffer of 10 mM HEPES (4-2-hydroxyethyl-1-piperazineethanesulfonic acid) and 50 mM NaCl was prepared using ultrapure water (Milli-Q reverse osmosis system, 18.2 mΩ·cm resistivity) to pH 7.4 and filtered with a 200 nm filter and used for all experiments.

Depletion addition

The polymer, being previously dissolved in the 10 mM HEPES 50 mM NaCl buffer, was mixed with the CSLB dispersion before deposition into the imaging chamber, after which the sample was again allowed to sediment for 30 minutes.

Confocal microscopy imaging

---

[1] Laboratory of Self-Organizing Soft Matter, Department of Chemical Engineering and Chemistry, Eindhoven University of Technology, P.O. Box 513, 5600 MB Eindhoven, The Netherlands

[2] Laboratory of Physical Chemistry, Department of Chemical Engineering and Chemistry, Eindhoven University of Technology, P.O. Box 513, 5600 MB Eindhoven, The Netherlands

[3] Institute for Complex Molecular Systems (ICMS), Eindhoven University of Technology, P.O. Box 513, 5600 MB Eindhoven, The Netherlands

The CSLBs prepared here are 3 μm in diameter and so sediment rapidly from solution, rendering the analysis of particle association in 3D impertinent. Therefore, we focus on imaging in *quasi*-2D. In order to be as systematic as possible in data collection, the sample preparation and imaging conditions were carefully controlled. Specifically, each CSLB dispersion examined was diluted to the required concentration with 10 mM HEPES and 50 mM NaCl buffer and sonicated for 30 minutes prior to pipetting into a μ-slide glass bottom well plate for imaging. To prevent scavenging of the lipid bilayer by the glass coverslide, the imaging chamber was passivated prior to imaging by incubation with 1 mg/ml solution of bovine serum albumin (BSA) for 1 hour. After rinsing with imaging chamber with buffer, each sample of CSLBs was allowed to deposit on the coverslip for 30 minutes before commencing imaging (ESI – Figure S.2). For accurate *quasi*-2D analysis of the colloidal interactions of CSLBs, a large statistical representation for each sample is required. Here, this requirement was met by using resonance and tile scanning to rapidly image a large number of regions of interest (ROI) and then compiled to render one large image. In this way, images of approximately 1000 μm × 1000 μm were collected by compiling >1000 individual tiles, consisting of CSLBs numbering in the range of 1000 – 30 000 particles depending on the dispersion concentration examined.

S.1 Self-Consistent Mean-Field Theory (SCFT)

Modelling CSLB interaction

We have previously described the use of Self-Consistent Mean-Field Theory (SCFT) to model the formation and composition of CSLBs, including the discretization of components [1]. Each chemical unit in the SCF computations is considered as taking up a single lattice unit, except for the phosphate group which takes five units arranged in a cross-like shape (see Figure S7 of Ref 1). The FH parameters, relative permeabilities and number of charges per monomer considered for the different chemical units defined as lattice beads used for the SCFT computations are given in Table 1.

Table 1. Overview of the Flory–Huggins interaction parameters χ_{ij}, relative permeabilities ϵ and charge per bead ν of the different chemical units modelled as lattice beads in SCFT. All these units fill a single lattice site, except for PO occupies which occupies 5 lattice units in a cross-like shape. The valency of N depends on whether it is charged or not. In DOPC, N is positively charged, whereas in DSPE–PEG$_{2000}$ it is uncharged.

		H_2O	**C**	**O**	**PO**	**N**	**Na**	**Cl**	**Si**
ϵ		80	2	1.5	80	7	10	10	5
ν/mon		0	0	0	-0.2	{1,0}	1	-1	-0.1
χ_{ij}	**H_2O**	0	1.6	-0.7	-1	0.5	0	0	1.0
	C		0	1.6	2	2	1.6	1.6	0
	O			0	0	0	-0.7	-0.7	0
	PO				0	0	-1	-1	0
	N					0	0.5	0.5	0
	Na						0	0	1.0
	Cl							0	1.0
	Si								0

To account for electrostatic interactions, the lattice site size b needs to be specified. We set b = 0.3 nm. All computations are conducted at a fixed salt concentration of 60 mM, which is converted to the appropriate volume fraction of ions in the bulk, which also impose electroneutrality of the total system. The lattice coordination number is set to Z = 6: we only consider a simple cubic lattice and conduct our calculations accounting for concentration gradients in one direction only. A description of the molecules involved in the computations is provided in Figure S7 of Ref 1.

The PEG (= PEO) chains were modeled as composed of freely-jointed chains composed of 'carbon' C units and 'oxygen' O units. Each EO monomer is described as units of two C's and one O unit with sequence O-C-C. Each monomeric unit has a molar mass of 44 g/mol. Hence the number of segments per PEO chain is computed from the molar mass of the chain divided by the molar mass of an EO unit (Table S1 in Ref 1).

Here SCFT is used to predict the strength and nature of SUV-SUV to CSLB-CSLB interactions. The SCFT lattice computations are based upon using the formalism developed by Scheutjens and Fleer [2–4]. To perform the computations we used the sfbox software developed by professor F.A.M. Leermakers and colleagues at Wageningen university, the Netherlands.

For a fixed surfactant bulk concentration determined from equilibrium with that of an isolated bilayer, two planar bilayers are brought closer together by varying the lattice size N_{lat} [5–7]. By monitoring the changes in the self-assembly equilibrium properties, interactions between self-assembled bilayers are obtained to mimic the interactions between vesicles. Particularly, we express the flat bilayer—flat bilayer interaction $W(h)$ per surface area as:

$$\frac{W(h)}{kT} = \sum_{i=1}^{N_{\mathrm{c}}} n_i^{\mathrm{exc}}(h)\mu_i(h) - n_i^{\mathrm{exc}}(\infty)\mu_i(\infty), \qquad \text{S.1}$$

with h the distance between the surfaces, N_{c} the number of components in the lattice (surfactant, ions, and solvent), n_i^{exc} are the excess numbers of compounds in the lattice (the aggregation number per bilayer cross-section), and μ_i their corresponding chemical potentials. Interactions are normalised with kT, with k Boltzmann's constant and T the absolute temperature. All quantities are directly extracted from the sfbox output. Here, N_{N} corresponds to the number of nearest neighbours. For a free-standing bilayer $N_{\mathrm{N}} = 1$ and $h = N_{\mathrm{lat}}$. We have checked that the computed interactions between two flat bilayers for bilayers formed in the centre of the lattice ($h = N_{\mathrm{lat}}$) or bilayers formed around the origin of the lattice ($h = 2N_{\mathrm{lat}}$) are in close agreement, yet the latter is a more stable numerical approach which is followed here. In case of DSPE-PEG$_{2000}$, the higher tendency of the PEGylated phospholipids to stay in solution produces slightly different results with the two different approaches.

We also use Equation S.1 for calculating the interactions between two infinite Si-planes in presence of the bilayers: the vesicle-mediated Si-Si interaction. When calculating these interactions we consider $N_{\mathrm{N}} = 1$ and $h = 2N_{\mathrm{lat}}$. The computations start at a lattice with $N_{\mathrm{lat}} = 300$, such that h_{max}, and the two vesicle-decorated Si surfaces do not interact with each other. In applying Equation 1 also in presence of charged surfaces, we assume the electrostatic repulsion between the Si surfaces is negligible compared to the energy variation originating from changes in the vesicles. Considering the high salt concentration accounted for, the electrostatic repulsion between the Si surfaces is screened within the domain of the SUV vesicles. Due to the high salt concentration considered, the Si-Si charge-charge repulsion is already screened within the domain of the vesicles

(Debye screening length $\kappa^{-1} \approx 1.23$ nm for a 60 mM salt in water; the vesicles have a thickness of ~ 5 nm as follows from experimental and SCF results). Therefore, this becomes a reasonable assumption.

We convert the interactions between two flat interfaces to interactions between the actual (colloidal) spheres (with radius a) by virtue of the Derjaguin approximation[8]:

$$W_s(h) = \pi a \int_h^{\infty} W(H) dH, \qquad \text{S.2}$$

with $W(H)$ the interaction between two flat surfaces. In the discrete lattice used, one needs to use the approximation $\mathrm{d}H = 2b$ as we only considered a single hard Si surface and replace Equation S.3 with its discrete version:

$$W_s(h) \approx 2b\pi a \sum_{h}^{h_{\max}} W(h) \qquad \text{S.3}$$

with $W(H)$ given in Equation S.1. We set the silica radius to $a = 1500$ nm (1.5 μm), according to the experimental values.

SCFT prediction of depletion interaction

Following the experimental results, we also considered the addition of non-adsorbing PEG chains to the vesicle-decorated Si surfaces. Consistent with the coarse-graining of the phospholipids, the free PEG polymer is considered as [C-C-O]$_m$ with m the number of repeating units [$m = \text{molar mass}/(\text{monomer molar mass})$]. As we focus on PEG with a molar mass of 100 kDa, $m = 2270$.

To compare with experiments we consider a (C-C-O) segment as the repeating unit with size b. Then the polymer overlap volume fraction ϕ^* follows as:

$$\phi^* = \frac{m\, b^3}{\frac{4\pi}{3} * R_g{}^3} \approx 0.012 \qquad \text{S.4}$$

for $m = 2270$. Since $\frac{\phi}{\phi^*} = \frac{c}{c^*}$ of the experimental system we can now study the effect of the added PEG.

From the experimental values, we get

$$\phi^{*,\mathrm{exp}} = \frac{c^*_{\mathrm{exp}}}{\rho} = 11.5[\mathrm{mg/ml}]/1130[\mathrm{mg/ml}] \approx 0.009 \qquad \text{S.5}$$

a value somewhat close to our theoretical estimation.

S.2 Synthesis of CSLBs

CSLBs were formed by first mixing 940 µL of 10 mM HEPES 50 mM NaCl with 60 µL of 50 mg/mL washed 3 µm silica particles and 360 µL of 1 mM solutions of phospholipid SUVs above the T_m of the phospholipids. DOPC and DPPC CSLBs were applied at room temperature, and 60 °C respectively. The suspension was mixed rapidly for 1 hr after which the CSLBs were washed 5 times with fresh buffer via centrifugation and redispersion. Finally, the CSLBs were sonicated for 1 hour, followed by storage in the fridge. All samples were used within two weeks.

S.3 Preparation of depletant

100 kDa poly(ethylene oxide) (Sigma Aldrich) was dissolved at 1.15 mg/ml in 10 mM HEPES 50 mM NaCl buffer (pH 7.4) and mixed for one hour followed by filtering through a 200 nm filter. All samples were used on the day of preparation.

S.4 Confocal microscopy imaging of spherically supported lipid bilayers

Sample preparation

All confocal imaging in this chapter was undertaken using µ-Slide 8 Well plates (ibidi, Gmbh). Prior to imaging, each well was rinsed using Milli-Q water and 400 µL of 1 mg/ml bovine serum albumin (BSA) solution applied for 1 hour. After1 hour, each well was washed 4 times with 10 mM HEPES, 50 mM NaCl buffer immediately prior to sample deposition.

All CSLB samples were diluted to the required concentration using 10 mM HEPES, 50 mM NaCl to a final volume of 300 µL, followed by 30 minutes of sonication to ensure dispersion. Immediately following sonication the same was pipetted into the imaging chamber and allowed to sediment for 30 minutes prior to imaging.

Clustering and pair interaction experiments by confocal microscopy

Confocal microscopy images were acquired using a 100× oil immersion objective on a Leica TCS-SP8 inverted microscope equipped with a 12000 Hz resonance scanner. Tile scanning of individual 512 × 512 pixel images using 2.5× zoom to render a pixel size of 0.091 µm. Large scale images were produced using the Leica LASX software merging function.

Confocal microscopy experimental design

Figure S.1 demonstrates the deposition of 3 µm CSLBs over 1 hour by bright-field microscopy. The number of particles in the field of view was monitored every 2 minutes showing a plateau occurring after 30 minutes (Figure S.1).

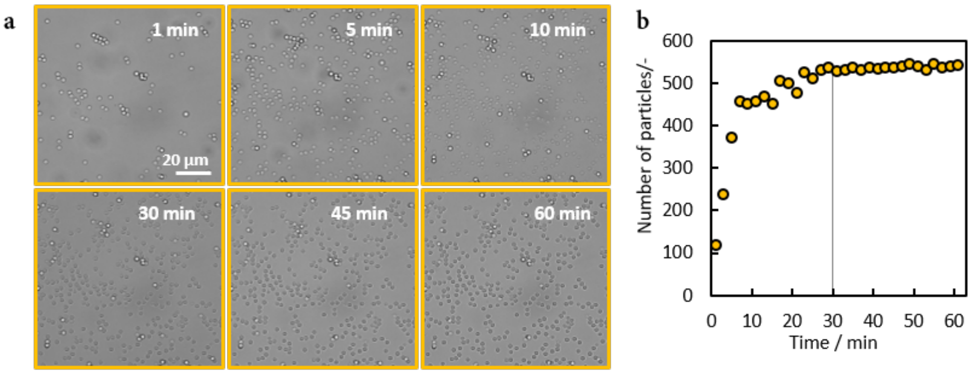

Figure S.1 – Detection of time required for sedimentation of CSLBs for optimisation of microscopy experiments. a) Sedimentation of DPPC CSLBs followed over time via bright field microscopy. b) Counts of the number of CSLBs detected in the field of view over 1 hour. A plateau is visible after 30 minutes (grey line).

S.5 Impact of particle concentration and calculation of area fraction

A wide range of CSLB concentrations were tested varying from dilute to concentrated (Figure S.2).

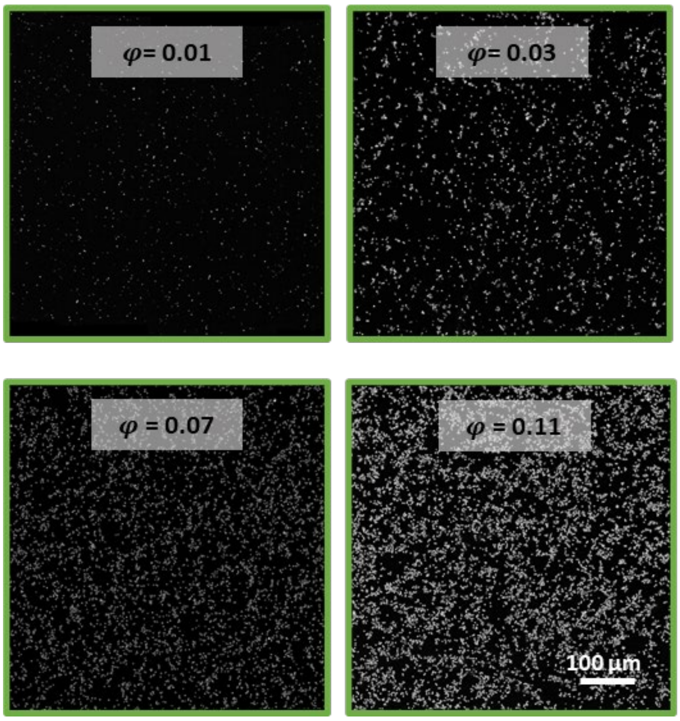

Figure S.2 – Confocal microscopy images of DPPC + 5%DSPE-PEG2000 CSLBs in quasi-2D ranging from dilute area fraction (φ = 0.01) to concentrated (φ = 0.11). CSLBs were allowed to sediment for 30 minutes prior to acquisition.

As the measurements were completed in *quasi*-2D, here we report the concentration of CSLBs in terms of area fraction φ:

$$\varphi = \frac{\pi\left(\frac{d}{2}\right)^2 N_\mathrm{p}}{XY} \qquad \text{S.6}$$

where d (µm) is the diameter of the particle, N_p is the number of particles detected in the image and XY (µm^2) is the area of the image. To ensure an accurate representation of the spatial configurations between the CSLBs mediated by the interactions between them, multiple dilutions and repeats of each experimental condition were performed. An average of 10 area fractions for each system were analysed. Importantly, experimental $g(r)$ values are extremely sensitive to the particle concentration, and so are only comparable between samples with closely matching area fractions.

S.6 Experimental determination of g(r)

Figure S.3. exemplifies the process of circle matching and cluster assignment for a single tile of a rendered image. First, the CSLBs were identified and counted using circle matching, the sensitivity of which was optimised for each individual image to limit the number of false positives and missed particles (Figure S.3.a.1).

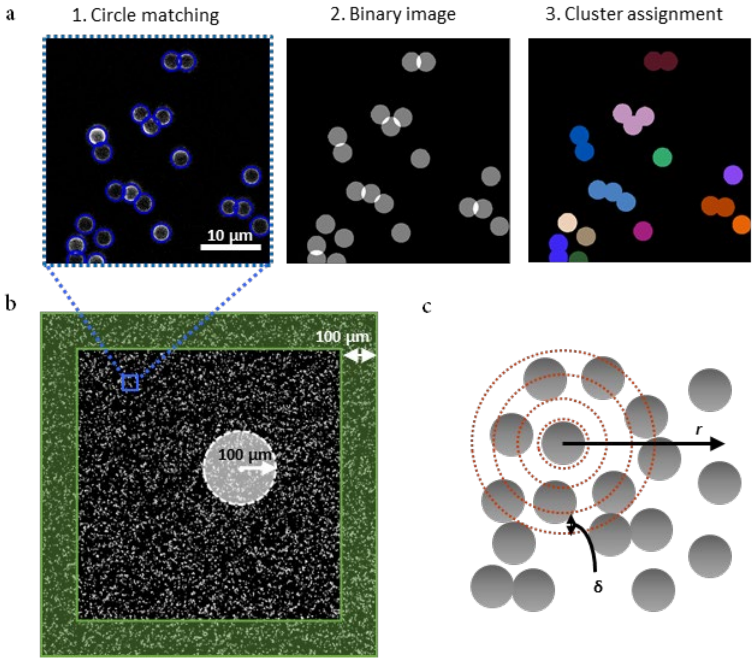

Figure S.3 – Tile scanning confocal microscopy images of CSLBs in *quasi*-2D analysed to quantify clustering and pair interactions. a) Confocal images are analysed by 1. CSLBs are identified by circle matching (blue circles) and particle centre x-y coordinates recorded, 2. creation of a binary image, 3. particles are assigned to a cluster on the criteria of pixel connectivity. Note – colours are randomly assigned. b) The centre to centre distance of each particle to all particles within a 100 µm radius is averaged over all particles and normalised to produce the radial distribution function $g(r)$. To eliminate truncation edge effects, the $g(r)$ of particles within the green area are not calculated, but do contribute to the $g(r)$ of particles within the black area. c) A representation of radial counting to determine the number of particles from a central particle, within a shell of thickness δ.

Next, the x-y coordinates of each particle centre were recorded in a matrix of particle-particle distances. To evaluate the cluster distribution within the sample, the identified particles were converted to a binary image (Figure S.3.a.2) and assigned to a cluster on the criteria of pixel connectivity to neighbouring particles. In Figure

S.3.a.3, the definition between clusters is apparent, where discrete clusters are demonstrated by random colour assignment. From this association, the distribution of CSLBs in certain cluster sizes can be obtained.

The probability density function describes the probability of finding a CSLB at a distance r from a central CSLB, within a circle which size is defined by r_{max}. Figure 1.b demonstrates this for r_{max} = 100 μm. To compute the *quasi*-2D probability density function from the experimental data we use the definition of $g(r)$ as:

$$g(r) = \frac{\rho(r)}{\overline{\rho}}, \qquad \text{S.7}$$

where the 2D effective particle density $\rho(r)$ (particles/μm^2) is normalised by the average particle density of the complete sample $\overline{\rho}$, (particles/μm^2). The average particle density is given by:

$$\overline{\rho} = \frac{N_{\mathrm{T}}}{XY}, \qquad \text{S.8}$$

where N_{T} is the total number of CSLBs in the image and XY is the total area of the image. To calculate the effective particle density, the localisation matrix of x-y coordinates and centre to centre distances of CSLBs was employed to create an individual histogram for each particle. Specifically, the number of CSLBs found within a shell of thickness δ as a function of distance from the central particle were counted, $N(r)$ (Figure S.3.c). Then, the histogram at each position was normalised by the shell area $2\pi r\delta$ to account for the trivial nature of more particles being found at larger r values, rendering the effective particle density:

$$\rho(r) = \frac{N(r)}{2\pi r\delta}. \qquad \text{S.9}$$

This is completed in a cyclic method and averaged to produce the mean $g(r)$ for the sample image. To avoid skewing of the $g(r)$ curve, the existence of edge effects originating from the truncation of the confocal images were considered. The edge effect occurs when particles that lie closer to the edge of the image (green area in Figure S.3.b) than the size of the maximum shell considered in $g(r)$ calculations, r_{max}. By excluding those particles, they were negated while still allowing them to contribute to the $g(r)$ of particles in the centre of the image (green and black areas, Figure S.3.b).

S.7 Impact of area fraction on g(r)

The theoretically maximum peak of a $g(r)$ as measured in 2D is determined by the area fraction of the system, and follows from Equation S.7:

$$g(d)_{\mathrm{max}} = \frac{\varphi_{\mathrm{max}}}{\varphi_{\mathrm{bulk}}}, \qquad \text{S.10}$$

where d is the diameter of the particle. Therefore, somewhat counterintuitively, the theoretically maximum $g(r)$ peak for attractive dilute systems is higher than that of a concentrated sample. If we consider that the theoretical maximum area fraction in the proximity of the central particles is $\varphi_{\mathrm{max}} \approx 0.9$, occurring for highly attractive systems, then for a dilute system where φ=0.01 then $g(d)_{\max}$ =90 (Figure S.2.a). Conversely, in a more concentrated system where φ=0.1 then $g(d)_{\max}$ =9 (Figure S.2.d).

S.8 Confirmation of g(r) analysis by analysis of close packed silica scaffold

To evaluate the accuracy of determining the $g(r)$, a scanning electron microscopy (SEM) image of the 3 µm silica spheres used to form the CSLBs was examined (Figure S.4). In this case, the sample of particles was dried for imaging and so the spheres display a close packed arrangement, allowing for comparison to other solid state systems [9]. To determine the influence of $r_{\max}$, values of were 10, 20 and 25 µm were considered (Figure S.4. b and c).

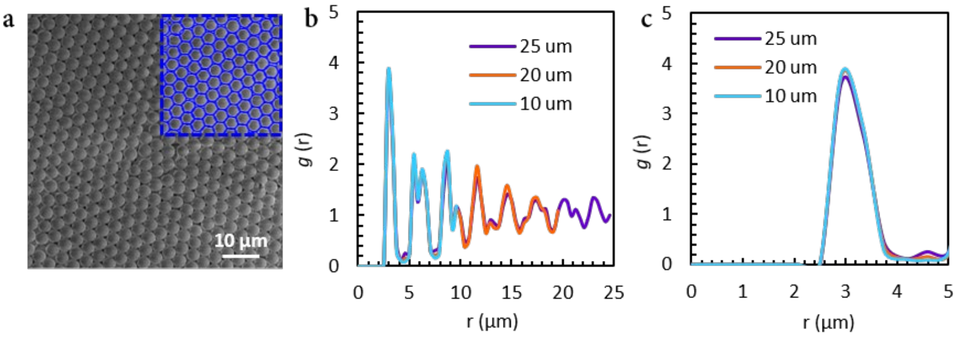

Figure S.4 – Probability density function, $g(r)$, analysis of dried 3 µm silica particles as imaged by SEM. a) SEM image. The inset shows the circle identification (blue circles). b) Probability density function calculated using $r_{\max}$ values of 25 µm, 20 µm and 10 µm. c) Zoom in on the first peak of the $g(r)$ curves shown in b).

The $g(r)$ curves in Figure S.4.b resulting from the analysis of Figure S.4.a demonstrate a characteristic shape for ordered close packed spheres [9, 10]. Firstly, $g(r) = 0$ for $r < d$, where d is the diameter of the particle as is expected for hard core excluded volume interactions. Then, there is the appearance of a sharp first peak near $r = d$, followed by a series of oscillations reflecting orders shells including well-defined peaks as r reaches multiples of d. Importantly, although it was not possible to reach large values of r due to the size of the image, the $g(r)$ can be seen to be tending towards 1 as r increases [11–14]. The splitting of the 2nd and 3rd peaks at $r = 6$ µm and $r = 9$ µm, respectively, indicates the solid nature of the system [9]. The $g(r)$ curves resulting from varying $r_{\max}$ are demonstrated to be essentially equivalent, suggesting a reproducible depiction of the statistical distribution of articles. The minor variation in peak height apparent in Figure S.4.c can be attributed to the difference in number of particles sampled in the considered circle indicating only a slight dependence of $g(r)$ on $r_{\max}$. Therefore, to analyse the $g(r)$ of CSLBs in large scale confocal images, the $r_{\max}$ was fixed at 100 µm.

S.11 Experimental depletion interactions

The polymer overlap concentration (c^*) quantifies the point at which a polymer solution moves from the dilute regime, where single polymer chains do not interact with one another, to the semi-dilute or entanglement regime. The overlap concentration is often described by:

$$c^* = \frac{3M_{\mathrm{p}}}{4\pi R_{\mathrm{g}}^3 N_{\mathrm{av}}}, \qquad \text{S.11}$$

Where M_p (g/mol) is the molar mass of the polymer, N_av is Avogadro's number and R_g (nm) is the radius of gyration of the polymer. Specifically, here we add 100 kDa polyethylene glycol as the depletant, where $R_\mathrm{g} \approx 12$ nm and so c^*=23 g/L [15]. The polymer overlap concentration gives the concentration beyond which the addition of extra polymer will start to have a less significant effect on the strength of depletion [16]. Here, we focus on concentrations corresponding to 0.05c^* and 0.1c^*, being 0.575 mg/ml and 1.15mg/ml respectively. The maximum strength of the attraction induced by the addition of PEG can be estimated by [17]:

$$\frac{W_{\mathrm{dep}}^{\mathrm{max}}}{kT} = -\frac{3}{2}\frac{c}{c^*}\frac{1}{\underline{q}} \qquad \text{S.12}$$

which is valid for $\underline{q} \lesssim 0.5$ where:

$$\underline{q} = \frac{R_\mathrm{g}}{a} \qquad \text{S.13}$$

where a is the CSLB radius. Therefore, for the present system W^{max} is estimated to be −10 kT and

−20 kT for 0.05c^* and 0.1c^* respectively. Note that for the highest free PEG concentration added, a repulsive contribution to the interaction between the CSLBs is found around an interparticle distance of 30 nm (Fig 4a). Adding high concentrations of depletants is known to lead to a repulsive contribution to the depletion interaction. This effect is most pronounced for hard spheres [18],. Upon increasing the free nonadsorbing polymer concentration such effects also appear [19]. This explains the repulsive contribution to the interaction potential in this case. It is noted however, that the attraction at shorter interparticle distances still overwhelms this weak repulsion.

References

1. Giakoumatos EC, Gascoigne L, Gumí-Audenis B, et al (2022) Impact of poly(ethylene glycol) functionalized lipids on ordering and fluidity of colloid supported lipid bilayers. Soft Matter 18:7569–7578. https://doi.org/10.1039/D2SM00806H

2. Scheutjens JMHM, Fleer GJ (1979) Statistical theory of the adsorption of interacting chain molecules. 1. Partition function, segment density distribution, and adsorption isotherms. J Phys Chem 83:1619–1635. https://doi.org/10.1021/j100475a012

3. Scheutjens JMHM, Fleer GJ (1980) Statistical theory of the adsorption of interacting chain molecules. 2. Train, loop, and tail size distribution. J Phys Chem 84:178–190. https://doi.org/10.1021/j100439a011

4. Fleer GJ, Cohen Stuart MA, Scheutjens JMHM, et al (1993) Polymers at Interfaces

5. García ÁG, Ianiro A, Tuinier R (2018) On the Colloidal Stability of Spherical Copolymeric Micelles. ACS Omega 3:17976–17985. https://doi.org/10.1021/acsomega.8b02548

6. Meijer LA, Leermakers FAM, Lyklema J (1995) Modeling the interactions between phospholipid bilayer membranes with and without additives. J Phys Chem 99:17282–17293. https://doi.org/10.1021/j100047a037

7. González García Á, Ianiro A, Beljon R, et al (2020) (Homo)polymer-mediated colloidal stability of micellar solutions. Soft Matter 16:1560–1571. https://doi.org/10.1039/C9SM01665A

8. González García Á, Nagelkerke MM., Tuinier R, Vis M (2020) Polymer-mediated colloidal stability: on the transition between adsorption and depletion. Adv Colloid Interface Sci 275:

9. Wang Z, Alsayed AM, Yodh AG, Han Y (2010) Two-dimensional freezing criteria for crystallizing colloidal monolayers. J Chem Phys 132:154501. https://doi.org/10.1063/1.3372618

10. Bergman M On the Phase Behaviour of Soft Matter: Understanding Complex Interactions via Quantitative Imaging

11. Yethiraj A, van Blaaderen A (2003) A colloidal model system with an interaction tunable from hard sphere to soft and dipolar. Nature 421:513–517. https://doi.org/10.1038/nature01328

12. Royall CP, Leunissen ME, Blaaderen a Van (2003) A new colloidal model system to study long-range interactions quantitatively in real space. J Phys Condens Matter 15:S3581–S3596. https://doi.org/10.1088/0953-8984/15/48/017

13. Ivell SJ, Dullens RPA, Sacanna S, Aarts DGAL (2013) Emerging structural disorder in a suspension of uniformly dimpled colloidal particles. Soft Matter 9:9361–9365. https://doi.org/10.1039/C3SM52059E

14. Hill TL (1986) An Introduction to Statistical Thermodynamics. Dover Publications

15. Tanaka S, Ataka M (2002) Protein crystallization induced by polyethylene glycol: A model study using apoferritin. J Chem Phys 117:3504–3510

16. Stenger PC, Isbell SG, Zasadzinski JA (2008) Molecular weight dependence of the depletion attraction and its effects on the competitive adsorption of lung surfactant. Biochim Biophys Acta - Biomembr 1778:2032–2040. https://doi.org/https://doi.org/10.1016/j.bbamem.2008.03.019

17. Lekkerkerker HNW, Tuinier R (2011) Colloids and the Depletion Interaction. Springer Science

18. Mao Y, Cates ME, Lekkerkerker HNW (1995) Depletion force in colloidal systems. Phys A Stat Mech its Appl 222:10–24. https://doi.org/https://doi.org/10.1016/0378-4371(95)00206-5

19. Semenov AN, Shvets AA (2015) Theory of colloid depletion stabilization by unattached and adsorbed polymers. Soft Matter 11:8863–8878. https://doi.org/10.1039/C5SM01365H